

Preclinical Activity of Nanoliposomal Irinotecan Is Governed by Tumor Deposition and Intratumor Prodrug Conversion

Ashish V. Kalra, Jaeyeon Kim, Stephan G. Klinz, Nancy Paz, Jason Cain, Daryl C. Drummond, Ulrik B. Nielsen, and Jonathan B. Fitzgerald

Abstract

A major challenge in the clinical use of cytotoxic chemotherapeutics is maximizing efficacy in tumors while sparing normal tissue. Irinotecan is used for colorectal cancer treatment but the extent of its use is limited by toxic side effects. Liposomal delivery systems offer tools to modify pharmacokinetic and safety profiles of cytotoxic drugs. In this study, we defined parameters that maximize the antitumor activity of a nanoliposomal formulation of irinotecan (nal-IRI). In a mouse xenograft model of human colon carcinoma, nal-IRI dosing could achieve higher intratumoral levels of the prodrug irinotecan and its active metabolite SN-38 compared with free irinotecan. For example, nal-IRI administered at doses 5-fold lower than free irinotecan achieved similar intratumoral exposure of SN-38 but with superior antitumor activity. Tumor response and pharmacokinetic modeling identified the duration for which concentrations of SN-38 persisted above a critical intratumoral threshold of 120 nmol/L as determinant for antitumor activity. We identified tumor permeability and carboxylesterase activity needed for prodrug activation as critical factors in achieving longer duration of SN-38 in tumors. Simulations varying tumor permeability and carboxylesterase activity predicted a concave increase in tumor SN-38 duration, which was confirmed experimentally in 13 tumor xenograft models. Tumors in which higher SN-38 duration was achieved displayed more robust growth inhibition compared with tumors with lower SN-38 duration, confirming the importance of this factor in drug response. Overall, our work shows how liposomal encapsulation of irinotecan can safely improve its antitumor activity in preclinical models by enhancing accumulation of its active metabolite within the tumor microenvironment. *Cancer Res*; 74(23); 7003–13. ©2014 AACR.

Introduction

Liposomal carriers have become clinically accepted in cancer therapy as delivery systems that can enhance the utility of existing anticancer drugs (1). The potential benefits of these macromolecular carriers include overcoming solubility issues for certain drug classes, protecting the drug from unwanted metabolism and extending the residence time in plasma and tissue. In particular, liposomes tend to preferentially accumulate in tumors as a result of an enhanced permeability and retention (EPR) effect. The EPR effect is attributed to the abnormal tumor vasculature permitting extravasation of macromolecules, as well as impaired lymphatic drainage that promote the retention of these molecules within the tumor microenvironment, thereby providing sustained release at the tumor site mimicking a metronomic dosing (2). Increased

tumor deposition via the EPR effect may also prevent drug resistance by overcoming the activity of multidrug resistant proteins (3, 4) and may offer possible means of improving safety aspects by reducing systemic exposure relative to tumor exposure (5). There are potential pharmacologic advantages of the EPR effect, particularly for antineoplastic agents that have to engage their target over a longer time period or have little binding activity; for example drugs of the camptothecin class with topoisomerase 1 enzyme (TOP1) as the primary target.

Irinotecan (CPT-11), a clinically approved camptothecin, is a prodrug that is activated by carboxylesterase (CES) enzymes, present primarily in liver and colon tissue to the active form, SN-38. (In the article, CPT-11 is used when referring to the prodrug levels in plasma or tumor samples following either free irinotecan or nal-IRI administration. SN-38 is used when referring to the active metabolite of CPT-11.) The active SN-38 can be subsequently inactivated through glucuronidation by members of the UDP glucuronosyltransferase family (6). The principal mechanism of action leading to cell death is through DNA damage after replication-fork collisions with transient drug-TOP1 cleavage complexes, thus emphasizing the time of drug exposure as important driver for cytotoxicity of camptothecins (7, 8). Recently, we described the development of a novel nanoliposomal formulation of irinotecan, nanoliposomal formulation of irinotecan (nal-IRI; also known as MM-398 or PEP02; ref. 9). nal-IRI features very high drug loading efficiency, a high drug payload, and marked *in vivo* drug retention that

Merrimack Pharmaceuticals, Inc., Cambridge, Massachusetts.

Note: Supplementary data for this article are available at Cancer Research Online (<http://cancerres.aacrjournals.org/>).

A.V. Kalra and J. Kim contributed equally to this article.

Corresponding Author: Jonathan B. Fitzgerald, Merrimack Pharmaceuticals, One Kendall Square, Suite B7201, Cambridge, MA 02139. Phone: 617-441-1029; Fax: 617-491-1386; E-mail: jfitzgerald@merrimackpharma.com

doi: 10.1158/0008-5472.CAN-14-0572

©2014 American Association for Cancer Research.

also stabilizes the active lactone configuration of irinotecan. The pharmacokinetic (PK) properties of the encapsulated irinotecan were dramatically altered in the plasma of female rats, with a 344× increase in the area under the curve (AUC), an 8.5× decrease in the volume of distribution, and a 39.6× increase in the half-life of the total drug. Pharmacokinetic analysis in a clinical study confirmed these performance characteristics of nal-IRI in patients (10).

Plasma drug concentrations cannot readily be translated into therapeutic effect; a sufficient amount of active therapeutic agent must be transported to the tumor site of action (i.e., be available for uptake by cancer cells) to observe favorable drug activity (11). The transport of macromolecules across the tumor vasculature is a complex process depending on vessel perfusion, surface area, and permeability, as well as tumor and drug characteristics. Several studies have used mathematical models to understand liposomal drug delivery within solid tumors (12, 13). Of particular interest is work done by Hendriks and colleagues (14), where the authors constructed a computational model to describe the parameters that affect the tumor delivery of pegylated liposomal doxorubicin, the first liposomal anticancer agent to receive clinical approval. The study concluded that liposome PK and tumor permeability to liposomes (tumor deposition) were the most important parameters controlling liposomal drug delivery to tumors.

In the case of nal-IRI, the complex metabolism (15) and mechanism of action (8, 16) of free irinotecan, in addition to the above-mentioned parameters, may play a role in the overall liposomal irinotecan delivery within tumors. In this study, we describe a systems pharmacology approach to identify critical parameters that differentiate nal-IRI from free irinotecan with regard to *in vivo* activity. A mechanistic tumor PK model was developed and trained to describe CPT-11 and SN-38 levels observed in plasma and tumor, following administration of either nal-IRI or free irinotecan in tumor xenografts. A model sensitivity analysis was performed to identify the critical parameters driving *in vivo* activity, which were then experimentally confirmed by measuring these factors in multiple cell line and patient-derived xenograft models. The findings in this study highlight critical parameters that could serve as potential biomarkers to identify cancer indications and patient populations with an increased likelihood of nal-IRI responsiveness.

Materials and Methods

Materials and nal-IRI preparation

nal-IRI was prepared as previously described (9) using a lipid composition of DSPC, cholesterol, and PEG-DSPE (3:2:0.015, mol:mol:mol), an initial drug-to-lipid ratio of 500 g drug/mol phospholipid, and extrusion through 0.1 μm polycarbonate filters. The resulting preparations displayed a particle size of 111 nm (with polydispersity index of 0.04), and a drug load of 473 mg irinotecan-HCl/mmol phospholipid. All lipids were obtained from Avanti Polar Lipids Inc. Irinotecan hydrochloride was purchased from the pharmacy. Acetic acid, methanol, and acetonitrile were from EMD Chemicals Inc. Water and trifluoroacetic acid (TFA) were from J.T. Baker. Fetal bovine serum was from Tissue Culture

Biologicals and phosphate-buffered saline (PBS) was purchased from Life Technologies.

Cell culture

Cell lines [HT-29 (colon), SK-ES-1 (Ewing's sarcoma), A549 (lung), LoVo (colon), MDA-MB-231 (breast)] were obtained from the ATCC, whereas A2780 cells (ovarian) was obtained from Sigma-Aldrich. Cells from the ATCC and Sigma were received in 2010. All cells were authenticated before receipt and were propagated for less than 6 months after resuscitation. Cultures are regularly tested for *Mycoplasma*. All cell lines were cultured in humidified CO₂ atmosphere at 37°C using media recommended by the manufacturer.

Pharmacokinetic and tissue biodistribution study

Five-week-old female NOD/SCID mice were purchased from Charles River Laboratory. The care and treatment of experimental animals were in accordance with the Institutional Animal Care and Use Committee guidelines. Subcutaneous tumors were established by injecting 10 million HT-29 cells into the right flank of mice. When the average tumor volume reached approximately 200 mm³, mice were randomized into groups ($n = 4$ /time point) that received a single intravenous (i.v.) dose of nal-IRI at 5, 10, 20, or 40 mg/kg. Following 1, 4, 8, 24, 48, 72, and 168 hours after a single dose, mice were sacrificed and perfused with PBS before harvest of tumor and other normal tissues.

Antitumor activity studies

Five-week-old female NOD/SCID mice were purchased from Charles River Laboratory. Subcutaneous tumors were established by injecting 10 million HT-29 and SK-ES-1 cells or 5 million A549 cells into the right flank of mice. Tumor growth was measured twice per week by calipers and calculated with formula: width² × length × 0.52. When the average tumor volume reached approximately 200 mm³, mice were randomized into treatment groups ($n = 5-8$ /group) that received weekly i.v. dose of PBS (control), free irinotecan (50 mg/kg), or nal-IRI at various doses ranging from 1.25 to 20 mg/kg.

Tumor growth inhibition (TGI) was calculated with formula:

$$\text{TGI}(\%) = \left[1 - \frac{(V_{\text{treated}}(d_{\text{final}}) - V_{\text{treated}}(d_0))}{(V_{\text{control}}(d_{\text{final}}) - V_{\text{control}}(d_0))} \right] \quad (\text{A})$$

where V_{treated} and V_{control} represent the volumes of tumor at a given time point following treatment with drug or PBS, and d_0 and d_{final} represent first day and final day of treatment, respectively.

Characterizing tumors from cell-line and patient-derived xenografts

The cell line-derived xenografts (HT-29, SK-ES-1, A549, MDA-MB-231, LoVo, AsPC-1, and A2780) were established as described above. The patient-derived tumor models [CTG-0062 (colorectal), CTG-0079 (colorectal), CTG-0252 (ovarian), CTG-0288 (pancreatic), CTG-0158 (lung), and CTG-0283 (pancreatic)] were established by Champions Oncology using their Champions TumorGraft (CTG) technology. When the

average tumor volume reached approximately 300 mm³, mice were randomized into treatment groups ($n = 4/\text{group}$) that received single i.v. dose of either PBS or nal-IRI at 10 mg/kg. Before tumor collection, intracardial perfusion was performed to remove the blood components from the tumor compartment. Briefly, a butterfly needle (23G) connected to a 10-mL syringe filled with PBS is inserted into the left ventricle. Inferior vena cava is cut and animal is perfused with 10-mL PBS (within 1–2 minutes). The control tumors were harvested 24 hours after PBS administration and used for the irinotecan activation assay, whereas the treated tumors were harvested either 24 or 72 hours following nal-IRI treatment and used for high-performance liquid chromatography (HPLC) analysis.

HPLC quantification of CPT-11 and SN-38

Tumor and normal tissues were analyzed for CPT-11 and SN-38 concentrations using a modification of the method previously described (9). Briefly, tissues were weighed and homogenized for 2 minutes in 20% w/v water using a Tissue-Lyser (Qiagen). The homogenates were extracted by mixing 0.1 mL homogenate with 0.9 mL 1% acetic acid/methanol followed by 10 seconds vortexing and placing at -80°C for 1 hour. The samples were centrifuged at 10,000 rpm for 10 minutes at room temperature and supernatants collected for HPLC analysis (Dionex). The samples and standards (CPT-11 and SN-38) were analyzed using a C18 reverse phase column (Synergi Polar-RP 80A 250 \times 4.60 mm 4 μm column). The drug metabolites were eluted running a gradient from 30% acetonitrile; 70% 0.1% TFA/H₂O to 68% acetonitrile; 32% 0.1% TFA/H₂O during a 13 minutes span at a flow rate of 1.0 mL/min. The

initial elute composition was restored after 14 minutes and continued for 6 minutes before the next injection. The CPT-11 peak was detected at approximately 7.7 minutes and the SN-38 peak eluted at approximately 8.4 minutes, using an in-line fluorescence detector excited at 372 nm and emitting at 556 nm.

Irinotecan activation assay

Tumor tissue lysates were prepared by homogenizing the tissue in 6% w/v 0.1 M Tris HCL/1% Triton X-100 solution (pH7.5) using a TissueLyser for 2 to 4 minutes. Protein concentration of lysates was measured using the BCA reagent (Thermo Scientific). Lysates (250 μg of protein) were mixed with an equal volume of 10 $\mu\text{mol/L}$ irinotecan and incubated at 37 $^{\circ}\text{C}$. Following 24 hours of incubation the reaction was terminated by adding an equal volume of 1% acetic acid/methanol and samples centrifuged at 10,000 rpm for 15 minutes. The supernatant was processed for HPLC quantification of CPT-11 and SN-38 as described above.

Statistical analysis

The statistical significance of differences between groups was analyzed with the one-way ANOVA test. Results were considered statistically significant at $P < 0.05$. The analysis was performed using GraphPad Prism 6.01.

Model development and simulation

Pharmacokinetic profiles of metabolites in plasma and tumor from free irinotecan and nal-IRI were described by using multi-compartmental models (Fig. 1B). The model equations are explained and summarized in the Supplementary

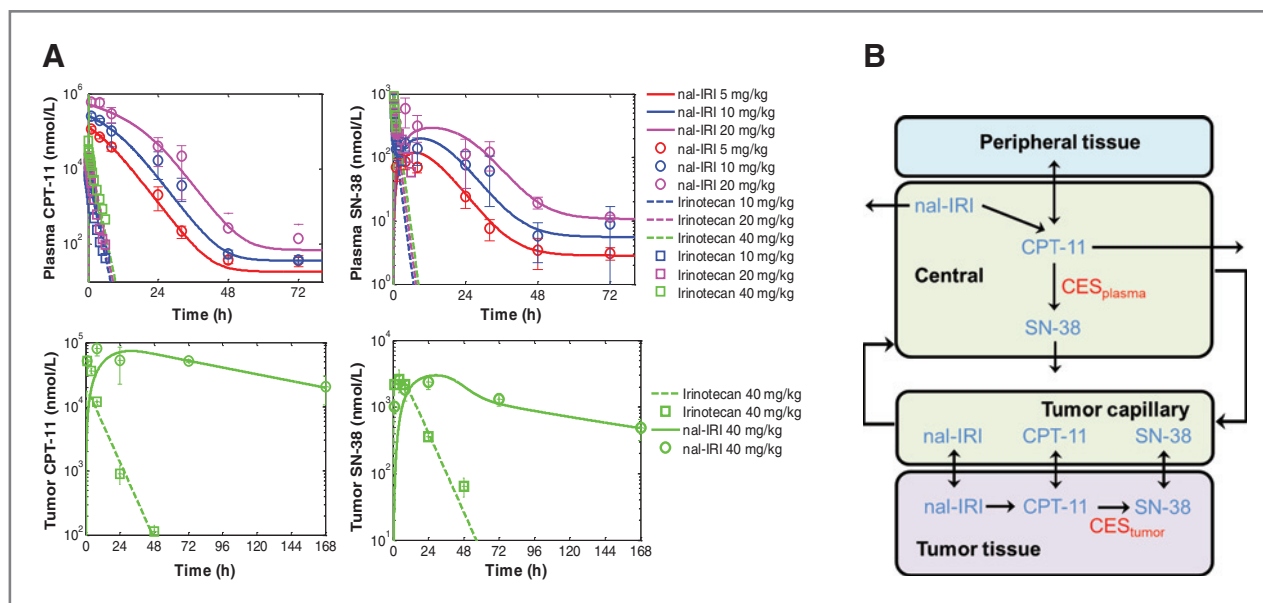


Figure 1. Pharmacokinetic profile of nal-IRI and free irinotecan. A, plasma and tumor PK of nal-IRI were compared with free irinotecan in HT-29 xenograft bearing mice. NOD/SCID mice bearing HT-29 tumors were treated with single i.v. dose of free irinotecan or nal-IRI. Plasma and tumors were collected at various intervals; CPT-11 and SN-38 were measured by HPLC analysis ($n = 4$ animals/time point). Plasma PK data for free irinotecan were taken from Kaneda and colleagues (35). Solid lines represent the model simulations for nal-IRI, whereas dashed lines represent the model simulations for free irinotecan. B, diagram of the mechanistic tumor pharmacokinetic model developed to describe the various steps in metabolism, pharmacokinetics and tumor deposition of nal-IRI.

Table 1. Summary of model parameters for plasma PK and tumor deposition models

| Name | Value | Units | Description | Reference |
|--|----------|----------|---|------------|
| Plasma PK model parameters | | | | |
| <i>For free irinotecan</i> | | | | |
| Cl_{CPT-11} | 1.222e-4 | L/min | Plasma clearance rate of CPT-11 | Estimated |
| Cl_{SN-38} | 2.138e-5 | L/min | Plasma clearance rate of SN-38 | Estimated |
| $k_{12,CPT-11}$ | 8.444e-5 | 1/min | Rate of CPT-11 transport from plasma to peripheral compartment | Estimated |
| $k_{21,CPT-11}$ | 4.213e-2 | 1/min | Rate of CPT-11 transport from peripheral to plasma compartment | Estimated |
| $k_{12,SN-38}$ | 2.656e-5 | 1/min | Rate of CPT-11 transport from plasma to peripheral compartment | Estimated |
| $k_{21,SN-38}$ | 3.44e-4 | 1/min | Rate of CPT-11 transport from peripheral to plasma compartment | Estimated |
| $V_{max,CES,p}$ | 2.263e-1 | nmol/min | Maximum rate coefficient for CES enzyme in plasma compartment | Estimated |
| $K_{m,CES,p}$ | 2.67e5 | nmol/L | Michaelis-Menten constant for CES enzyme in plasma compartment | Estimated |
| V_p | 9.46e-5 | L | Volume of plasma compartment | Estimated |
| V_{ph} | 0.02 | L | Volume of peripheral compartment | Fixed (14) |
| <i>For nal-IRI</i> | | | | |
| $Cl_{nal-IRI}$ | 1.87e-7 | L/min | Plasma clearance rate of nal-IRI | Estimated |
| Cl_{CPT-11} | 1.634e-5 | L/min | Plasma clearance rate of CPT-11 | Estimated |
| Cl_{SN-38} | 2.957e-6 | L/min | Plasma clearance rate of SN-38 | Estimated |
| $k_{12,CPT-11}$ | 1.619e-4 | 1/min | Rate of CPT-11 transport from plasma to peripheral compartment | Estimated |
| $k_{21,CPT-11}$ | 5.349e-7 | 1/min | Rate of CPT-11 transport from peripheral to plasma compartment | Estimated |
| $V_{max,Release,p}$ | 8.443e-6 | nmol/min | Maximum rate coefficient for CPT-11 release from nal-IRI in plasma compartment | Estimated |
| $K_{m,Release,p}$ | 2.04 | nmol/L | Michaelis-Menten constant for CPT-11 release from nal-IRI in plasma compartment | Estimated |
| $V_{max,CES,p}$ | 5.943e-2 | nmol/min | Maximum rate coefficient for CES enzyme in plasma compartment | Estimated |
| $K_{m,CES,p}$ | 1.198e-5 | nmol/L | Michaelis-Menten constant for CES enzyme in plasma compartment | Estimated |
| V_p | 1.12e-3 | L | Volume of plasma compartment | Estimated |
| V_{ph} | 0.02 | L | Volume of peripheral compartment | Fixed (14) |
| Tumor deposition model parameters | | | | |
| Q_{tumor} | 2.119e-6 | L/min | Blood flow rate to tumor | (14) |
| $PS_{nal-IRI}$ | 7.858e-5 | L/min/kg | Tissue permeability coefficient of nal-IRI | Estimated |
| PS_{CPT-11} | 1.851e-3 | L/min/kg | Tissue permeability coefficient of CPT-11 | Estimated |
| PS_{SN-38} | 2.687e-2 | L/min/kg | Tissue permeability coefficient of SN-38 | Estimated |
| $\sigma_{nal-IRI}$ | 3.181e-3 | | Tissue-capillary partition coefficient of nal-IRI | Estimated |
| σ_{CPT-11} | 5.24e-1 | | Tissue-capillary partition coefficient of CPT-11 | Estimated |
| σ_{SN-38} | 2.109e-1 | | Tissue-capillary partition coefficient of SN-38 | Estimated |
| $k_{Release,t}$ | 1.681e-4 | 1/min | Rate coefficient for CPT-11 release from nal-IRI in tumor tissue compartment | Estimated |
| $V_{max,CES,t}$ | 2.17e-2 | nmol/min | Maximum rate coefficient for CES enzyme in tumor tissue compartment | Estimated |
| $K_{m,CES,t}$ | 2.3e-6 | nmol/L | Michaelis-Menten constant for CES enzyme in tumor tissue compartment | Estimated |
| V_{cap} | 7e-7 | L | Volume of tumor capillary compartment | (14) |
| V_t | 1e-5 | L | Volume of tumor tissue compartment | Fixed |

Data. The models were built and implemented using Simbiology toolbox in MATLAB 8.2 (The MathWorks).

Results

nal-IRI displays a prolonged exposure in both plasma and tumor compared with free irinotecan

The pharmacokinetic profiles of the prodrug CPT-11 and its active metabolite SN-38 were measured in plasma and tumors following administration of either free irinotecan or nal-IRI (Fig. 1A). At similar doses of both free irinotecan and nal-IRI, the CPT-11 and SN-38 plasma levels cleared rapidly from circulation within 8 hours after free irinotecan injection,

whereas the levels of CPT-11 and SN-38 following nal-IRI administration were persistent and remained in circulation for over 50 hours. An approximately 10-fold higher plasma CPT-11 peak level was observed with nal-IRI as compared with free irinotecan. However, the plasma peak level of SN-38 achieved with nal-IRI was 10-fold lower compared with free irinotecan, probably due to the ability of the lipid bilayer to protect the conversion of prodrug CPT-11 to SN-38 by the systemic CES enzyme present in mouse models (17). Administration of free irinotecan resulted in the clearance of greater than 90% of CPT-11 from tumors within 24 hours; however, following nal-IRI administration, CPT-11 levels persisted above

10,000 nmol/L levels for 168 hours. Similar peak levels of SN-38 were achieved with both free irinotecan and nal-IRI in HT-29 tumors, though a prolonged SN-38 exposure for up to 168 hours (measured as the AUC from 0 to 168 hours) was achieved with nal-IRI as compared with less than 48 hours tumor exposure with free irinotecan. In summary, CPT-11 and SN-38 were still present in tumors at 168 hours following nal-IRI administration, though both CPT-11 and SN-38 had cleared from plasma.

Tumor SN-38 duration drives *in vivo* activity

We developed a mechanistic PK model to identify the determinants that may differentiate the plasma and tumor PK profiles between free irinotecan and nal-IRI (Fig. 1B). The experimental PK data were used to estimate the optimal model

parameters (Table 1) fitting the model simulations within the standard deviations of *in vivo* PK profiles of both CPT-11 and SN-38 (Fig. 1A). As the *in vitro* cytotoxic effects of irinotecan on tumor cells is dependent on the concentration and the time of exposure of cells to active metabolite SN-38 (7, 8), we sought to understand if the overall plasma and tumor SN-38 exposure predicts the *in vivo* activity of both nal-IRI and free irinotecan. The trained model determined that a 5-fold higher dose of free irinotecan (50 mg/kg) was required to achieve similar SN-38 exposure in both plasma and tumor as compared with nal-IRI (10 mg/kg; Fig. 2A). The TGI of HT-29 xenograft model at these equal exposure doses, was significantly greater with nal-IRI (~110%) treatment as compared with free irinotecan (~40%), despite the 5-fold lower total dose administered (*, $P < 0.05$,

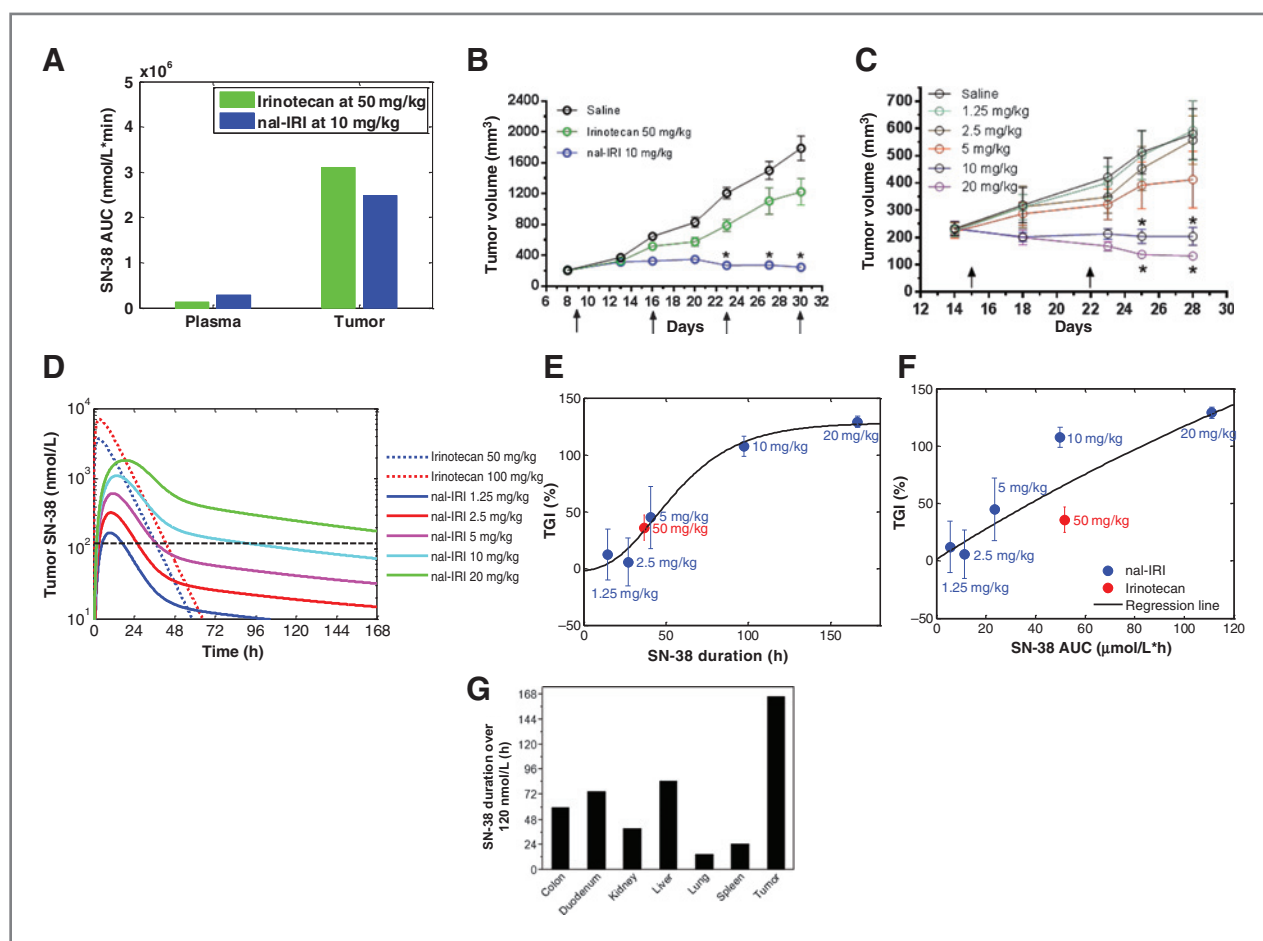


Figure 2. Relation of nal-IRI *in vivo* activity to tumor SN-38 duration. A, model predictions for similar SN-38 AUC in plasma and tumor following free irinotecan (50 mg/kg) and nal-IRI (10 mg/kg) administration. B, tumor response observed in HT-29 xenograft following weekly administration (arrows) of 50 mg/kg free irinotecan and 10 mg/kg nal-IRI ($n = 8$ /group). The tumor volumes for nal-IRI (10 mg/kg) were significantly lower (*, $P < 0.05$) compared with saline and irinotecan groups (one-way ANOVA test). C, tumor response in HT-29 xenografts following weekly administration (arrows) of various nal-IRI doses ($n = 5$ /group). The tumor volumes for nal-IRI (10 mg/kg) and nal-IRI (20 mg/kg) groups were significantly lower (*, $P < 0.05$) compared with saline tumors on day 25 and day 28 (one-way ANOVA test). D, model simulations were used to compare tumor SN-38 concentration following the administration of varying doses of free irinotecan or nal-IRI. Black dashed line represents threshold concentration of 120 nmol/L to determine tumor SN-38 duration. E and F, TGI(%) achieved by nal-IRI and free irinotecan treatment in HT-29 xenografts were compared with the tumor SN-38 duration above 120 nmol/L (E) and SN-38 AUC (F) at varying doses of nal-IRI or free irinotecan. Solid lines represent nonlinear regression lines based on five parameter logistic curve fitting. G, the SN-38 duration over a threshold of 120 nmol/L was computed from the pharmacokinetic profiles of SN-38 in tumor and normal tissues following 20 mg/kg of nal-IRI.

one-way ANOVA test; Fig. 2B). In addition, other studies have shown no additional HT-29 TGI at the maximum tolerated dose of free irinotecan (100 mg/kg; ref. 18). To identify a dose level of nal-IRI that gave comparable *in vivo* activity to 50 mg/kg free irinotecan, we performed a dose escalation study in the HT-29 xenograft model (Fig. 2C). nal-IRI at 5 mg/kg showed partial inhibition of tumor growth (~40% TGI) that was comparable with 50 mg/kg free irinotecan, whereas 10 mg/kg and 20 mg/kg nal-IRI showed significant (*, $P < 0.05$, one-way ANOVA test) TGI compared with saline (~110%–130% TGI). Furthermore, we have previously tested control liposomes (that have comparable composition with nal-IRI except for the absence of irinotecan, the active pharmaceutical ingredient) and did not observe any TGI (data not shown).

The intratumor SN-38 concentrations achieved from 50 to 100 mg/kg doses of free irinotecan and 1.25, 2.5, 5, 10, and 20 mg/kg doses of nal-IRI were then simulated using the trained mechanistic PK model (Fig. 2D). Although a nal-IRI dose of 5 mg/kg achieved similar TGI as 50 mg/kg free irinotecan, the tumor SN-38 AUC and peak levels were approximately 2-fold and 6-fold lower respectively for nal-IRI as compared with free irinotecan. Furthermore, we noted at these doses both drugs were able to maintain the tumor SN-38 concentration above 120 nmol/L for the same duration of approximately 40 hours. To determine if the tumor SN-38 concentration impacts *in vivo* activity, we used the tumor SN-38 concentration of 120 nmol/L as a threshold. We also determined the duration for which the various doses of nal-IRI or free irinotecan could maintain the tumor SN-38 concentration above 120 nmol/L, hereon referred to as "tumor SN-38 duration." A sigmoidal relationship between TGI (%) and tumor SN-38 duration (Fig. 2E) was observed for both nal-IRI and free irinotecan ($R^2 = 0.62$). However, when comparing TGI (%) with tumor SN-38 AUC (Fig. 2F) the relationship was

less significant ($R^2 = 0.45$), due to the lower TGI (%) achieved by 50 mg/kg free irinotecan compared with 10 mg/kg nal-IRI. We also observed longer SN-38 duration in tumors (>100 hours) compared with normal tissues (<72 hours; Fig. 2G and Supplementary Fig. S1).

Identification of liposome tumor permeability and local tumor activation as critical determinants for tumor SN-38 duration

A local sensitivity analysis on the model parameters was performed to identify processes impacting the tumor SN-38 duration (Supplementary Data). In response to the administration of free irinotecan (50 mg/kg), the tumor SN-38 duration was relatively insensitive to most model parameters (Fig. 3A), suggesting the inability of free irinotecan to modulate it. In contrast, several model parameters were found to significantly impact tumor SN-38 duration following the administration of nal-IRI (10 mg/kg; Fig. 3B). The sensitive parameters for nal-IRI can be classified into three different categories: (i) PK, rate of breakdown of liposomes in blood (Release rate in blood, $V_{\max, \text{Release,p}}$), (ii) activation of prodrug CPT-11 to SN-38 by CES enzyme (CES activity in tumor; $V_{\max, \text{CES,t}}$ and blood; $V_{\max, \text{CES,p}}$), and (iii) liposome uptake within tumors, that is, nal-IRI tumor deposition (nal-IRI tumor permeability, $PS_{\text{nal-IRI}}$). Among these parameters, the release rate in plasma negatively affected tumor SN-38 duration due to a decrease in the overall systemic exposure of nal-IRI. CES enzyme activity, particularly from tumor CES (local tumor activation of irinotecan) and nal-IRI permeability (tumor deposition), positively affected the tumor SN-38 duration. To assess the identifiability of parameter estimates, log likelihood profiling was performed for the sensitive parameters, $V_{\max, \text{CES,t}}$ and $PS_{\text{nal-IRI}}$ (19). The confidence intervals suggested that both parameters were precisely estimated (Supplementary Fig. S2).

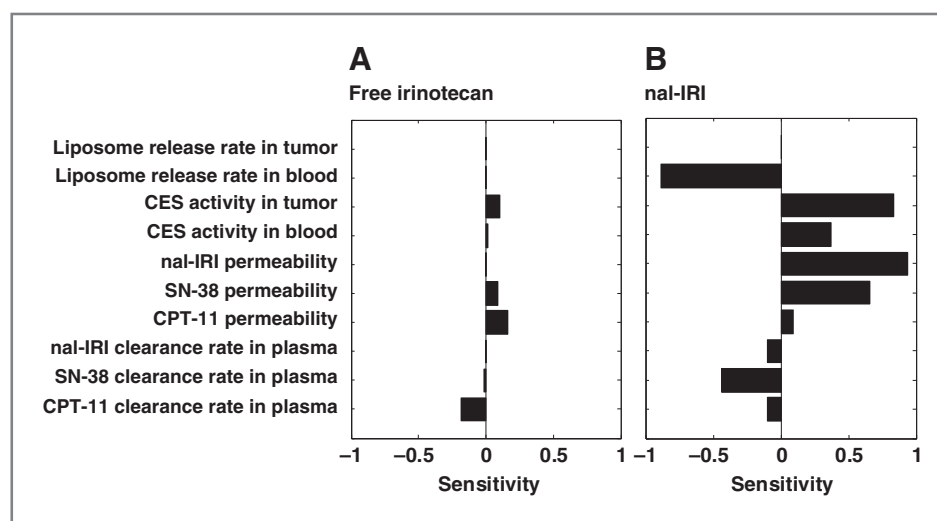


Figure 3. Model parameters impacting tumor SN-38 duration. Sensitivity analyses for free irinotecan (A) and nal-IRI (B) were performed on key model parameters that are responsible for plasma clearance, tissue deposition and metabolic reactions. Parameters whose values were not estimated in this study, including compartment volumes and tumor blood flow, were excluded from the analysis. The doses of free irinotecan (50 mg/kg) and nal-IRI (10 mg/kg) that achieved similar SN-38 plasma and tumor exposure were used for sensitivity analysis. The model parameters were modulated by 10% and their effect on tumor SN-38 duration was determined as a sensitivity index (Supplementary Equation S6).

Biologic variability and simulated perturbation of nal-IRI tumor deposition and local activation

To determine the biologic relevance of these sensitive parameters toward driving tumor SN-38 duration (namely nal-IRI tumor deposition and local tumor activation of irinotecan), the parameters were measured in a panel of 13 xenograft models. We used the total CPT-11 concentrations in tumors as a surrogate for nal-IRI tumor deposition as model simulations based on nal-IRI pharmacokinetics showed that majority of CPT-11 in plasma and tumor was encapsulated and protected within the liposomes and less than 10% was available as free CPT-11 (Supplementary Fig. S3). The intratumor con-

centrations of CPT-11 varied substantially across the tumor panel (Fig. 4A). The tumor models from cell-lines displayed overall higher levels of prodrug CPT-11 deposition (from 5,000–15,000 ng/g) as compared with patient-derived tumor models (1,000–2,000 ng/g). In addition, a high degree of variability was observed between individual tumors within the same xenograft model (66% average coefficient of variation). Model simulations were used to test the effect of altering nal-IRI tumor deposition on tumor SN-38 duration (Fig. 4B). By decreasing the nal-IRI permeability parameter to zero, which simulates an impermeable tumor microenvironment, the tumor SN-38 duration of approximately 100 hours achieved

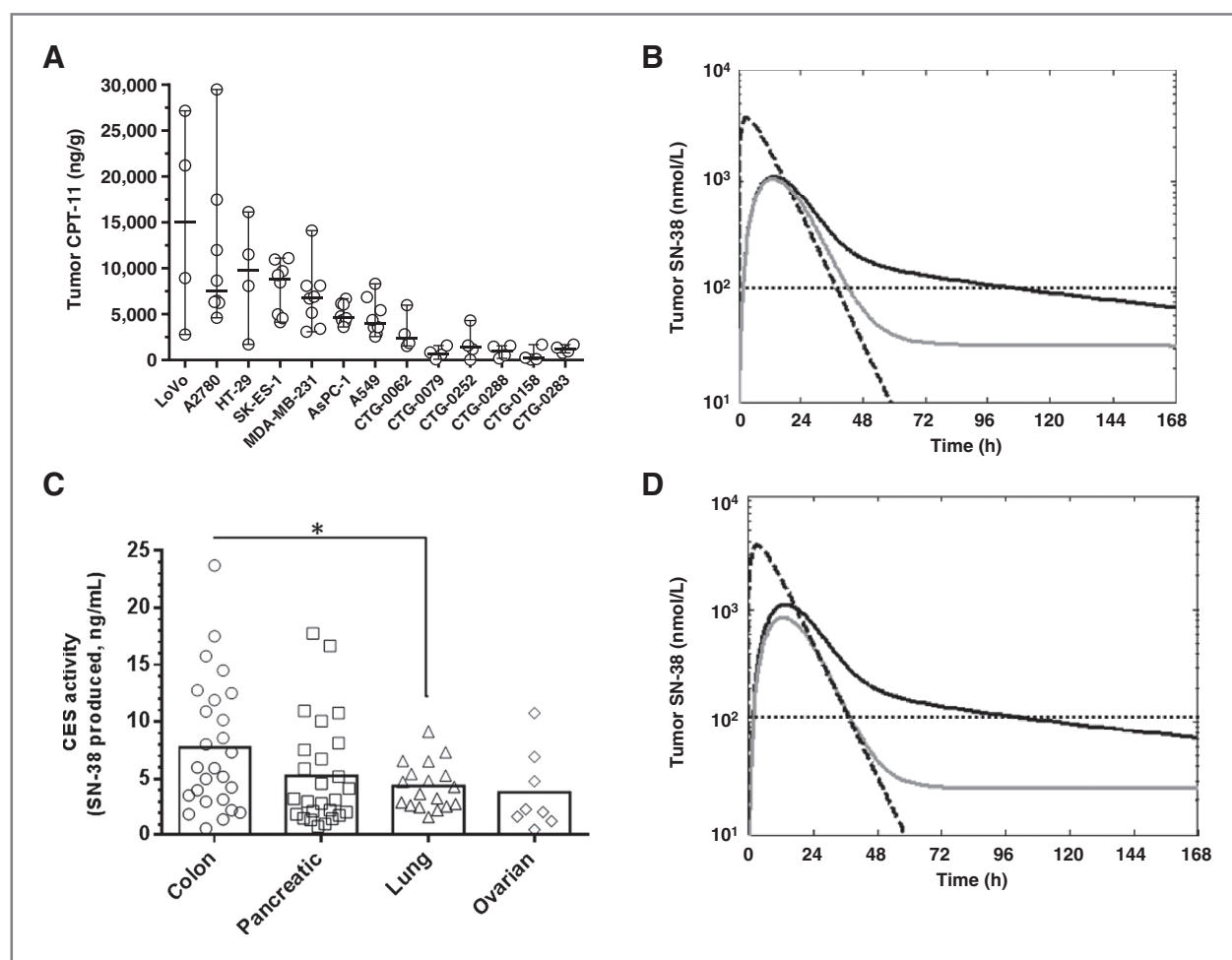


Figure 4. *In vivo* variability in nal-IRI tumor deposition and local activation. A, intratumor CPT-11 concentrations were measured across cell-line-derived (HT-29, SK-ES-1, A549, MDA-MB-231, LoVo, AsPC-1, and A2780) and patient-derived (CTG-0062, CTG-0079, CTG-0252, CTG-0288, CTG-0158, and CTG-0283) tumor models. Tumor-bearing mice were administered a single i.v. dose of 10 mg/kg nal-IRI and tumors excised 24 hours later. CPT-11 concentrations were determined in the tumor lysates using HPLC analysis as described in Materials and Methods ($n = 4-8$ tumors/model). B, the effect of nal-IRI permeability on tumor SN-38 concentrations was simulated by reducing the nal-IRI permeability parameter $PS_{nal-IRI}$ to zero. The simulated tumor SN-38 concentrations were compared at the equal exposure doses of 10 mg/kg nal-IRI and 50 mg/kg free irinotecan. Black solid line, nal-IRI (10 mg/kg) with base $PS_{nal-IRI}$. Gray solid line, nal-IRI (10 mg/kg) with zero $PS_{nal-IRI}$. Black dashed line, free irinotecan (50 mg/kg). Dotted line, threshold concentration of 120 nmol/L CES activity (C) for 80 patient-derived xenograft tumors across different indications was determined using *ex vivo* irinotecan activation assay. Tumor lysates (250 μ g of protein) from untreated mice was incubated with free irinotecan (5 μ mol/L) for 24 hours at 37°C and the amount of SN-38 produced was measured with HPLC analysis (*, $P < 0.05$; t test). D, the effect of knocking out tumor CES activity on tumor SN-38 duration was simulated by reducing the tumor CES parameter $V_{max,CES,t}$ to zero. The simulated tumor SN-38 concentrations were compared at the equal exposure doses of 10 mg/kg nal-IRI and 50 mg/kg free irinotecan. Black solid line, nal-IRI 10 mg/kg with base $V_{max,CES,t}$. Gray solid lines, nal-IRI 10 mg/kg with zero $V_{max,CES,t}$. Black dashed line, free irinotecan 50 mg/kg with base $V_{max,CES,t}$. Dotted line, threshold concentration of 120 nmol/L.

with 10 mg/kg nal-IRI was substantially reduced to approximately 50 hours and approached the levels observed with 50 mg/kg free irinotecan. Taken together, these results suggest that the tumor deposition of nal-IRI is highly tumor specific and will dramatically impact tumor SN-38 duration.

To determine the degree to which local tumor activation of irinotecan varied in human tumors, we measured CES activity using an *ex vivo* assay in a panel of 80 patient-derived tumors. The tumor lysates varied in their ability to activate prodrug irinotecan and produce SN-38 (1–25 ng/mL SN-38 produced), suggesting a high degree of variability in local tumor activation of irinotecan across indications. A significant difference in local tumor activation of irinotecan was observed between colon and lung tumors ($P < 0.05$). However, there was no significant difference between other indications, which may be due to high variability observed within each indication (Fig. 4C). The impact of varying the tumor CES activity on tumor SN-38 duration was evaluated by simulating a knockout of tumor CES enzyme (Fig. 4D). In the absence of local tumor activation, tumor SN-38 duration with nal-IRI (10 mg/kg) decreased from approximately 100 to 40 hours, similar to that achieved by free irinotecan (50 mg/kg).

nal-IRI tumor deposition and local activation collectively predict tumor SN-38 duration

The relative contribution of nal-IRI tumor deposition and local tumor activation on tumor SN-38 duration was evaluated using model simulations. On the basis of the findings from the sensitivity analysis (Fig. 3B), nal-IRI permeability ($PS_{\text{nal-IRI}}$) and tumor CES activity ($V_{\text{max,CES,t}}$) values were used to create a map relating these parameters to tumor SN-38 duration following nal-IRI administration (Fig. 5A). Model simulations predicted a concave relationship, where the tumor SN-38 duration is dependent upon both the tumor permeability and the tumor CES activity. The tumor SN-38 duration could be increased by either increasing the $PS_{\text{nal-IRI}}$ or $V_{\text{max,CES,t}}$ (white arrows) and the maximum tumor SN-38 duration of 168 hours was only

reached with CES activity at 0.025 nmol/min and tumor permeability at 1.5E–4 L/min/kg.

To experimentally test the model predictions, we used the same panel of 13 xenograft models to measure the tumor concentrations of CPT-11 (as a surrogate for tumor deposition, Supplementary Fig. S4A); tumor SN-38 concentrations (as a surrogate for tumor SN-38 duration; Supplementary Fig. S4B) and CES activity (for local tumor activation of irinotecan). The experimental data supported the model simulations, confirming that the SN-38 concentration within tumors was dependent on both the tumor CPT-11 concentration and tumor CES activity (Fig 5B). All tumor models with high CPT-11 concentration >2,000 ng/mL or high CES activity > 5 ng/mL displayed high tumor SN-38 concentrations ("red") ranging from 25 to 125 ng/mL (Supplementary Table S2). In certain tumor models, one of the parameters contributed predominantly toward higher SN-38 concentrations (black arrows). A2780 and SK-ES-1 tumors displayed high tumor SN-38 concentrations of 97 ng/mL and 127 ng/mL respectively (Supplementary Table S2), which was mainly due to high CPT-11 concentrations (>2,000 ng/mL), whereas in other tumor models (CTG-0062 and AsPC-1) the CES activity (>5 ng/mL) was the dominant factor contributing toward high tumor SN-38 concentrations. Further tumor models with the lowest tumor SN-38 concentrations ranging from 5 to 12 ng/mL ("blue"), including several patient-derived tumor models (boxed area) also displayed lower tumor CPT-11 concentrations (<2,000 ng/mL) and CES enzyme activity (<5 ng/mL).

Tumor SN-38 duration correlates with nal-IRI *in vivo* activity

In vivo tumor response studies were performed in three tumor models in which different tumor SN-38 durations had been observed (as indicated by tumor SN-38 concentration at 72 hours) to determine the impact of tumor SN-38 duration on *in vivo* activity of nal-IRI. The tumor volumes observed for both HT-29 (Fig. 6A) and SK-ES-1 (Fig. 6B) models were significantly

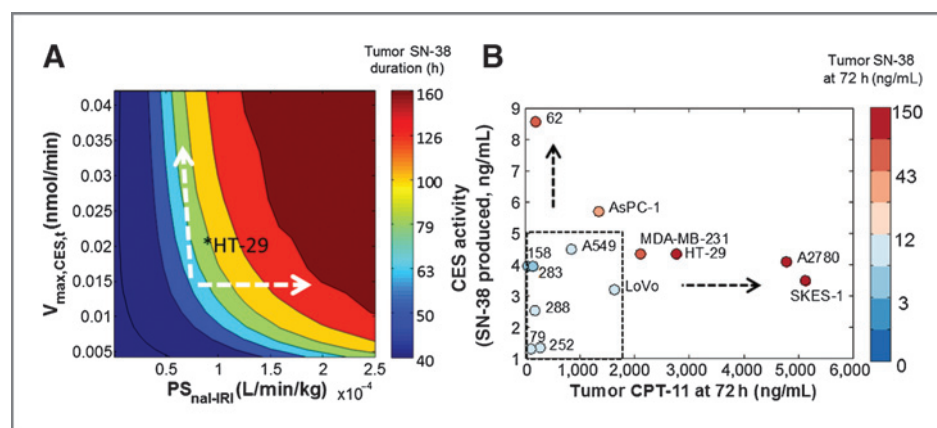


Figure 5. nal-IRI tumor deposition and local activation impacts tumor SN-38 duration. A, the effect of changing tumor CES activity and nal-IRI permeability parameters (arrows) on tumor SN-38 duration (color-coded in hours) in tumors was simulated. The optimal parameter values for HT-29 were marked with the symbol ***. B, experimental data in tumor xenograft models showing the impact of tumor CPT-11 and CES activity on tumor SN-38 concentrations. Tumor CES activity (as surrogate for local tumor activation of irinotecan) and tumor CPT-11 concentration at 72 hours (as surrogate for tumor deposition) for different xenograft models were plotted and color-coded on the basis of their SN-38 concentrations in the tumor 72 hours after nal-IRI (each data point represents median of $n = 4-8$ tumors). Dotted arrows, dependence of tumor SN-38 concentrations on tumor CPT-11 concentration and CES activity.

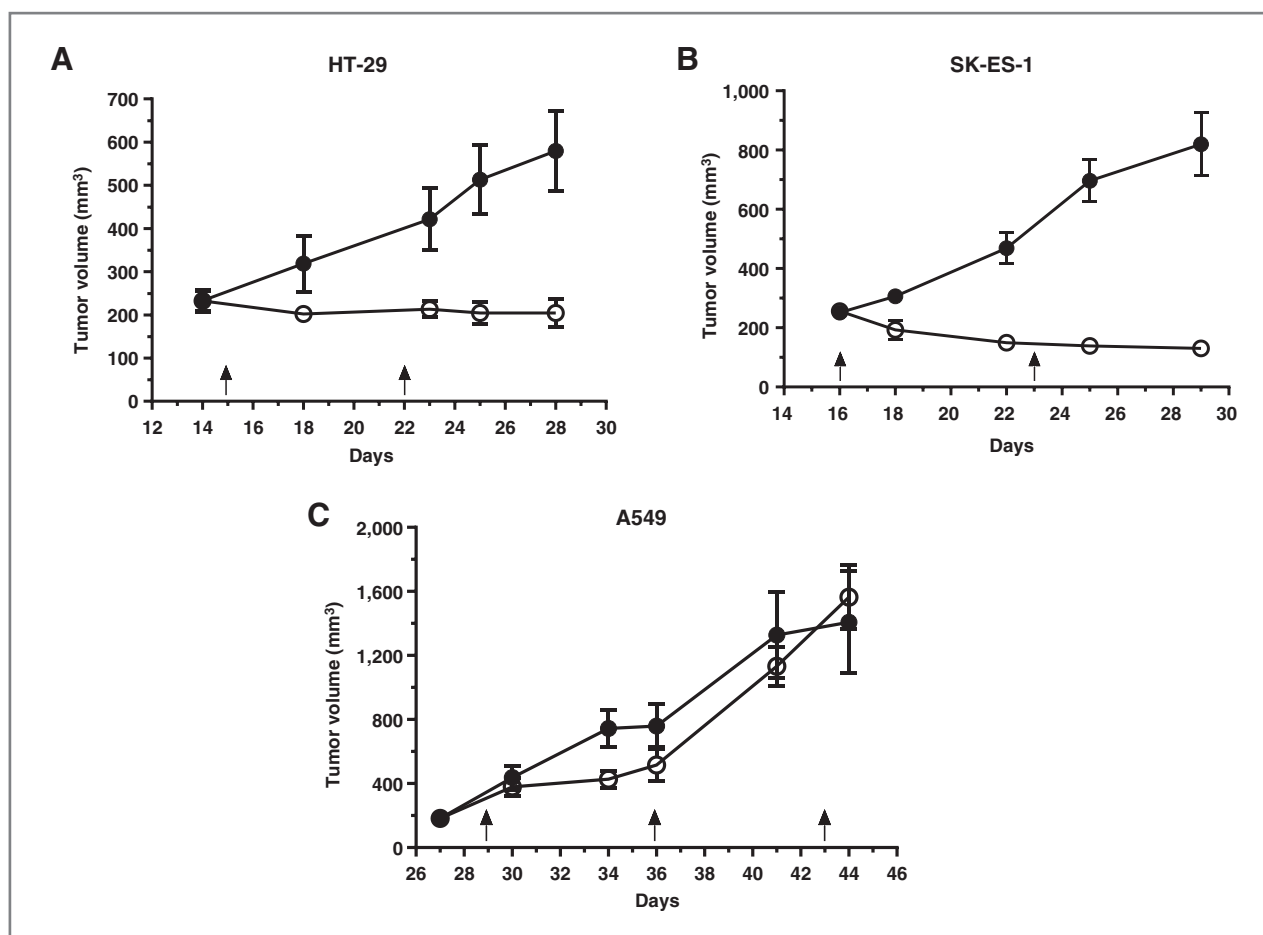


Figure 6. *In vivo* tumor response for nal-IRI. NOD/SCID mice were inoculated with HT-29; colon (A), SK-ES-1; Ewing's (B) and A549; lung (C) cell lines. Tumor-bearing mice were randomized when the tumor volume was approximately 200 mm³. Each group received weekly i.v. dose (arrows) of either saline (●) or 10 mg/kg dose of nal-IRI (○). Tumor volumes were measured twice per week ($n = 5-10$ animals/group).

lower ($P < 0.05$) following 10 mg/kg nal-IRI as compared with untreated tumors. In both these models, tumor regression was observed immediately after the first dose and was sustained through the course of the study. A549 tumors achieved lower SN-38 tumor levels (Fig. 4A) and did not respond to nal-IRI treatment (Fig. 6C). Interestingly, both A549 and HT-29 cells displayed similar *in vitro* sensitivity to SN-38 with IC₅₀ values of 53 and 44 nmol/L, respectively (20). In summary, nal-IRI induced stronger responses (~100%TGI) in tumor models that had higher tumor SN-38 duration (>~100 hours).

Discussion

The nal-IRI formulation dramatically alters the pharmacologic properties of irinotecan as well as its active metabolite, SN-38 (9). In this study, we identified a pharmacologic parameter—namely, tumor SN-38 duration—as a driver of irinotecan-based *in vivo* activity and propose biomarkers that can impact tumor SN-38 duration achieved by nal-IRI. Our study indicates that nal-IRI can completely inhibit tumor growth compared with free irinotecan, despite administering doses that achieve similar SN-38 exposure (measured as the AUC). Instead, the duration of prolonged exposure of SN-38 within tumors

achieved by nal-IRI was shown to be a major pharmacologic determinant for *in vivo* activity in mice.

Several studies have shown improved *in vitro* cytotoxic activity of SN-38 when cells are exposed to drug for longer duration (21). The *in vitro* cell doubling time for HT-29 cells is approximately 20 hours (21), whereas *in vivo* the tumor volume doubles (Fig. 2B) at a slower rate (~8–9 days). In addition, at a given time only 35 to 50% of cells are in the S-phase of cell cycle wherein the maximum cytotoxicity of free irinotecan has been observed (21). Thus, to exert maximum cytotoxic effects across different cell-cycle phases, the cells have to be exposed to free irinotecan across multiple cell cycles. Our *in vivo* study confirms these findings as the free irinotecan is rapidly cleared from plasma and tumor tissue (tumor SN-38 duration of approximately 40 hours), thereby not allowing sufficient time for tumor cells to be exposed to SN-38 (for only 2 cell-cycle doubling time) as compared with more than 5 cell-cycle doubling times with nal-IRI (tumor SN-38 duration for >100 hours). Thus the extended exposure of tumor cells to SN-38, which is achieved by nal-IRI, can contribute toward the enhanced cytotoxicity as compared with free irinotecan.

We observed higher tumor concentrations of CPT-11 and SN-38 at 168 hours following administration of nal-IRI. In contrast, the peak plasma concentrations of SN-38 was lower with nal-IRI as compared with free irinotecan, suggesting that most of the CPT-11 from nal-IRI remains inside the liposomes and is protected from systemic conversion as described with free irinotecan (17). In addition, prolonged SN-38 duration from nal-IRI administration was observed only in tumors and much less in normal tissues, suggesting that toxicity might not be exacerbated by nal-IRI treatment. The preferential accumulation of nal-IRI in tumors as compared with normal tissues can be attributed to the EPR effect, where the leaky vasculature in tumor facilitates the extravasation of liposomal nanoparticles and the defective lymphatic drainage helps increase the retention within tumor (1, 2). Thus, with the EPR effect, nal-IRI creates a large depot of CPT-11 only in tumors thereby prolonging tumor SN-38 duration. In contrast, free irinotecan can easily be transported in and out of the tissues with a short plasma half-life, resulting in minimal SN-38 duration in tumors.

The enhanced *in vivo* activity of nal-IRI as compared with free irinotecan was attributed to the ability of nal-IRI to extend the tumor SN-38 duration. Sensitivity analysis identified two key determinants that impact the ability of nal-IRI to extend tumor SN-38 duration—(i) nal-IRI tumor deposition, as measured by the extent of prodrug CPT-11 deposition within tumors and (ii) nal-IRI local activation, from prodrug CPT-11 to SN-38 facilitated by the local tumor CES enzyme. The experimental data, in this study supported the importance of each of these determinants. We observed high degree of variability in the overall nal-IRI tumor deposition across the 13 xenograft models that were tested. Several studies have highlighted a role for tumor permeability, tumor perfusion, and stromal matrix in limiting the delivery of therapeutic agents into tumors (22). In our model simulations, when the nal-IRI tumor permeability was decreased to zero, the benefit of higher tumor SN-38 duration with nal-IRI was negatively impacted and reduced to levels simulated for free irinotecan. We also observed that the tumors with lower nal-IRI deposition had considerable lower SN-38 tumor levels. These data are consistent with other findings suggesting that a dense tumor stroma can impede drug permeability and limit drug delivery within tumors (23, 24).

Use of tumor CES activity as a cellular parameter for predicting free irinotecan response had limited success both in preclinical (25, 26) and clinical studies.(27). Through the sensitivity analysis performed in this study, we identified CES activity as a critical parameter for nal-IRI activity. Tumor models that displayed high ability to activate CPT-11, achieved high tumor SN-38 concentrations despite limited deposition of CPT-11, thus suggesting the importance of local tumor CES enzyme expression in facilitating longer SN-38 exposure following nal-IRI administration. In fact, others have shown that *in vitro* and *in vivo* activity of free irinotecan can be enhanced by overexpressing of CES enzyme in tumor cells (28, 29). In addition to tumor cells expressing CES enzyme (30), other components of the extracellular matrix such as tumor-associated macrophages (TAMs) express CES1 enzyme and play a role in CPT-11 activation (31). In fact, we performed *in vitro*

studies that confirmed the ability of TAMs to hydrolyze CPT-11 to SN-38 (Supplementary Fig. S5). Thus our data suggests the extended tumor PK achieved by nal-IRI provides high local depot of prodrug CPT-11 for prolonged time, thus allowing for activation by tumor CES enzymes. Collectively our data provides rational for investigating tumor CES enzyme activity as a potential marker for nal-IRI activity.

Pharmacogenetic and pharmacodynamic markers such as TOP1 have shown limited correlations with free irinotecan response (6, 32–34). In addition to the intrinsic sensitivity of tumor cells to SN-38, our data indicate that the duration for which tumor cells are exposed to SN-38 (tumor SN-38 duration) also plays a critical role in driving treatment response to irinotecan. Tumor models with extended SN-38 duration (HT-29, SK-ES-1) showed robust *in vivo* response to nal-IRI, whereas A549 with shorter tumor SN-38 duration did not respond to therapy. The fact that *in vitro* sensitivity of both HT-29 and A549 to SN-38 is very similar (20) corroborates the finding that the duration of SN-38 is driving the tumor response.

In conclusion, our data demonstrate that nal-IRI enhances the pharmacokinetic profile of tumor SN-38, prolonging tumor exposure to SN-38 compared with free irinotecan, and therefore has the potential for therapeutic effect in human cancers. Liposome permeability and CES activity were the critical factors that emerged from model simulation of tumor SN-38 duration, which were experimentally shown to vary across and within tumor indications. Thus, translational research exploring the utility of tumor liposome permeability and local activation of irinotecan as biomarkers for nal-IRI clinical activity is warranted.

Disclosure of Potential Conflicts of Interest

D.C. Drummond and J.B. Fitzgerald have ownership interest (including patents) in Merrimack Pharmaceuticals, Inc. No potential conflicts of interest were disclosed by the other authors.

Authors' Contributions

Conception and design: A.V. Kalra, J. Kim, S.G. Klinz, D.C. Drummond, U.B. Nielsen, J.B. Fitzgerald

Development of methodology: A.V. Kalra, J. Kim, S.G. Klinz

Acquisition of data (provided animals, acquired and managed patients, provided facilities, etc.): A.V. Kalra, N. Paz, J. Cain

Analysis and interpretation of data (e.g., statistical analysis, biostatistics, computational analysis): A.V. Kalra, J. Kim, D.C. Drummond, J.B. Fitzgerald

Writing, review, and/or revision of the manuscript: A.V. Kalra, J. Kim, S.G. Klinz, D.C. Drummond, U.B. Nielsen, J.B. Fitzgerald

Administrative, technical, or material support (i.e., reporting or organizing data, constructing databases): J. Kim, N. Paz

Study supervision: A.V. Kalra, J.B. Fitzgerald

Acknowledgments

The authors thank Sharlene Adams and Arnold Sengooba for their contributions to the *in vivo* studies; Bart Hendriks for his feedback on PK modeling; Dimitri Kirpotin for the scientific discussions; and Eliel Bayever for critical review of the article.

Grant Support

This research was funded by Merrimack Pharmaceuticals, Inc.

The costs of publication of this article were defrayed in part by the payment of page charges. This article must therefore be hereby marked *advertisement* in accordance with 18 U.S.C. Section 1734 solely to indicate this fact.

Received March 4, 2014; revised July 21, 2014; accepted August 10, 2014; published OnlineFirst October 1, 2014.

References

- Drummond DC, Meyer O, Hong K, Kirpotin DB, Papahadjopoulos D. Optimizing liposomes for delivery of chemotherapeutic agents to solid tumors. *Pharmacol Rev* 1999;51:691–743.
- Maeda H. Tumor-selective delivery of macromolecular drugs via the EPR effect: background and future prospects. *Bioconjug Chem* 2010;21:797–802.
- Mamot C, Drummond DC, Hong K, Kirpotin DB, Park JW. Liposome-based approaches to overcome anticancer drug resistance. *Drug Resist Updat* 2003;6:271–9.
- Petitprez A, Poindessous V, Ouaret D, Regairaz M, Bastian G, Guérin E, et al. Acquired irinotecan resistance is accompanied by stable modifications of cell cycle dynamics independent of MSI status. *Int J Oncol* 2013;42:1644–53.
- Papahadjopoulos D, Gabizon A. Targeting of liposomes to tumor cells *in vivo*. *Ann N Y Acad Sci* 1987;507:64–74.
- Marsh S, Hoskins JM. Irinotecan pharmacogenomics. *Pharmacogenomics* 2010;11:1003–10.
- Pommier Y. Topoisomerase I inhibitors: camptothecins and beyond. *Nat Rev Cancer* 2006;6:789–802.
- Pommier Y. DNA topoisomerase I inhibitors: chemistry, biology, and interfacial inhibition. *Chem Rev* 2009;109:2894–902.
- Drummond DC, Noble CO, Guo Z, Hong K, Park JW, Kirpotin DB. Development of a highly active nanoliposomal irinotecan using a novel intraliposomal stabilization strategy. *Cancer Res* 2006;66:3271–7.
- Roy AC, Park SR, Cunningham D, Kang YK, Chao Y, Chen LT, et al. A randomized phase II study of PEP02 (MM-398), irinotecan or docetaxel as a second-line therapy in patients with locally advanced or metastatic gastric or gastro-oesophageal junction adenocarcinoma. *Ann Oncol* 2013;24:1–7.
- El-Kareh AW, Secomb TW. Theoretical models for drug delivery to solid tumors. *Crit Rev Biomed Eng* 1997;25:503–71.
- Uziely B, Jeffers S, Isacson R, Kutsch K, Wei-Tsao D, Yehoshua Z, et al. Liposomal doxorubicin: antitumor activity and unique toxicities during two complementary phase I studies. *J Clin Oncol* 1995;13:1777–85.
- Harashima H, Tsuchihashi M, Iida S, Doi H, Kiwada H. Pharmacokinetic/pharmacodynamic modeling of antitumor agents encapsulated into liposomes. *Adv Drug Deliv Rev* 1999;40:39–61.
- Hendriks BS, Reynolds JG, Klinz SG, Geretti E, Lee H, Leonard SC, et al. Multiscale kinetic modeling of liposomal doxorubicin delivery quantifies the role of tumor and drug-specific parameters in local delivery to tumors. *CPT Pharmacometrics Syst Pharmacol* 2012;1:e15.
- Smith NF, Figg WD, Sparreboom A. Pharmacogenetics of irinotecan metabolism and transport: an update. *Toxicol In Vitro* 2006;20:163–75.
- Holm C, Covey JM, Kerrigan D, Pommier Y. Differential requirement of DNA replication for the cytotoxicity of DNA topoisomerase I and II inhibitors in Chinese hamster DC3F cells. *Cancer Res* 1989;49:6365–8.
- Morton CL, Iacono L, Hyatt JL, Taylor KR, Cheshire PJ, Houghton PJ, et al. Activation and antitumor activity of CPT-11 in plasma esterase-deficient mice. *Cancer Chemother Pharmacol* 2005;56:629–36.
- Azrak RG, Cao S, Slocum HK, Tóth K, Durrani FA, Yin M, et al. Therapeutic synergy between irinotecan and 5-fluorouracil against human tumor xenografts. *Clin Cancer Res* 2004;10:1121–9.
- Raue A, Kreutz C, Maiwald T, Bachmann J, Schilling M, Klingmüller U, et al. Structural and practical identifiability analysis of partially observed dynamical models by exploiting the profile likelihood. *Bioinformatics* 2009;25:1923–9.
- Shoemaker RH. The NCI60 human tumour cell line anticancer drug screen. *Nat Rev Cancer* 2006;6:813–23.
- Goldwasser F, Bae I, Valenti M, Torres K, Pommier Y. Topoisomerase I-related parameters and camptothecin activity in the colon carcinoma cell lines from the National Cancer Institute anticancer screen. *Cancer Res* 1995;55:2116–21.
- Jain RK, Stylianopoulos T. Delivering nanomedicine to solid tumors. *Nat Rev Clin Oncol* 2010;7:653–64.
- Olive KP, Jacobetz MA, Davidson CJ, Gopinathan A, McIntyre D, Honess D, et al. Inhibition of Hedgehog signaling enhances delivery of chemotherapy in a mouse model of pancreatic cancer. *Science* 2009;324:1457–61.
- Neesse A, Michl P, Frese KK, Feig C, Cook N, Jacobetz MA, et al. Stromal biology and therapy in pancreatic cancer. *Gut* 2011;60:861–8.
- Jansen WJ, Zwart B, Hulscher ST, Giaccone G, Pinedo HM, Boven E. CPT-11 in human colon-cancer cell lines and xenografts: characterization of cellular sensitivity determinants. *Int J Cancer* 1997;70:335–40.
- Pavillard V, Agostini C, Richard S, Charasson V, Montaudon D, Robert J. Determinants of the cytotoxicity of irinotecan in two human colorectal tumor cell lines. *Cancer Chemother Pharmacol* 2002;49:329–35.
- Pavillard V, Charasson V, Laroche-Clary A, Soubeyran I, Robert J. Cellular parameters predictive of the clinical response of colorectal cancers to irinotecan. A preliminary study. *Anticancer Res* 2004;24:579–85.
- Danks MK, Morton CL, Pawlik CA, Potter PM. Overexpression of a rabbit liver carboxylesterase sensitizes human tumor cells to CPT-11. *Cancer Res* 1998;58:20–2.
- Kojima A, Hackett NR, Ohwada A, Crystal RG. *In vivo* human carboxylesterase cDNA gene transfer to activate the prodrug CPT-11 for local treatment of solid tumors. *J Clin Invest* 1998;101:1789–96.
- Xu G, Zhang W, Ma MK, McLeod HL. Human carboxylesterase 2 is commonly expressed in tumor tissue and is correlated with activation of irinotecan. *Clin Cancer Res* 2002;8:2605–11.
- Igarashi M, Osuga J, Uozaki H, Sekiya M, Nagashima S, Takahashi M, et al. The critical role of neutral cholesterol ester hydrolase 1 in cholesterol removal from human macrophages. *Circ Res* 2010;107:1387–95.
- Braun MS, Richman SD, Quirke P, Daly C, Adlard JW, Elliott F, et al. Predictive biomarkers of chemotherapy efficacy in colorectal cancer: results from the UK MRC FOCUS trial. *J Clin Oncol* 2008;26:2690–8.
- Alagoz M, Gilbert DC, El-Khamisy S, Chalmers AJ. DNA repair and resistance to topoisomerase I inhibitors: mechanisms, biomarkers and therapeutic targets. *Curr Med Chem* 2012;19:3874–85.
- Gilbert DC, Chalmers AJ, El-Khamisy SF. Topoisomerase I inhibition in colorectal cancer: biomarkers and therapeutic targets. *Br J Cancer* 2012;106:18–24.
- Kaneda N, Nagata H, Furuta T, Yokokura T. Metabolism and pharmacokinetics of the camptothecin analogue CPT-11 in the mouse. *Cancer Res* 1990;50:1715–20.

Cancer Research

The Journal of Cancer Research (1916–1930) | The American Journal of Cancer (1931–1940)

Preclinical Activity of Nanoliposomal Irinotecan Is Governed by Tumor Deposition and Intratumor Prodrug Conversion

Ashish V. Kalra, Jaeyeon Kim, Stephan G. Klinz, et al.

Cancer Res 2014;74:7003-7013. Published OnlineFirst October 1, 2014.

Updated version Access the most recent version of this article at:
doi:[10.1158/0008-5472.CAN-14-0572](https://doi.org/10.1158/0008-5472.CAN-14-0572)

Supplementary Material Access the most recent supplemental material at:
<http://cancerres.aacrjournals.org/content/suppl/2014/10/02/0008-5472.CAN-14-0572.DC1>

Cited articles This article cites 35 articles, 14 of which you can access for free at:
<http://cancerres.aacrjournals.org/content/74/23/7003.full#ref-list-1>

Citing articles This article has been cited by 9 HighWire-hosted articles. Access the articles at:
<http://cancerres.aacrjournals.org/content/74/23/7003.full#related-urls>

E-mail alerts [Sign up to receive free email-alerts](#) related to this article or journal.

Reprints and Subscriptions To order reprints of this article or to subscribe to the journal, contact the AACR Publications Department at pubs@aacr.org.

Permissions To request permission to re-use all or part of this article, use this link
<http://cancerres.aacrjournals.org/content/74/23/7003>.
Click on "Request Permissions" which will take you to the Copyright Clearance Center's (CCC) Rightslink site.